EJGE

Analysis of Stress Distribution around a Wellbore Drilled in Tight Sandstone Formations during Gas Drilling

Xu Yang

College of Oil and Gas engineering,
Southwest Petroleum University, Chengdu 610500, China
e-mail: yangxuzq@sina.com

Yingfeng Meng

College of Oil and Gas engineering,
Southwest Petroleum University, Chengdu 610500, China
e-mail: cwctmyf@swpu.edu.cn

Gao Li

College of Oil and Gas engineering,
Southwest Petroleum University, Chengdu 610500, China
e-mail: lgmichael@263.net

Hanfeng Tang

Sichuan Kehong Acer Oil and Gas Engineering Co., Ltd, Chengdu 610213, China

Liang Wang

Southwest Oil and Gas Field Company Engineering Technology Research Institute, Guanghan 618300, China

ABSTRACT

Gas drilling has been proven to be an effective means of increasing penetration rate and minimizing formation damage. Field cases in Tarim basin, western China, show the great advantage of gas drilling in drilling efficiency enhancement. However, wellbore instability caused by gas production from unexpected gas pay zone is always inevitable, which restricts the further application of gas drilling. A dual poroelastic model for fractured tight sandstone is developed to quantify the non-Darcy gas flow and tight sandstone deformation. The model separately accommodates gas flow and transport in tight sandstone matrix and fracture, then matrix/fracture porosity and permeability models are implemented into the coupled gas flow and deformation model. The effect of gas production on the evolution of permeability and stress of fractured tight sandstone is evaluated, together with its influence on stress distribution of overlying mudstone. Results reveal that tight sandstone may undergo an exfoliation mode of failure as a result of negative effective radial stress in the vicinity of wellbore. Gas production tends to increase the effective radial and tangential stresses in tight sandstone, suggesting enhanced wellbore stability with respect to tensile failure. The results also show sudden changes of total radial and tangential stresses at the lithology interface. The total tangential stress in the overlying mudstone tends to be largely increased by lithology variation. The increased shear stress may lead to wellbore instability of overlying mudstone, and gas production further increases the potential for shear failure of overlying mudstone.

KEYWORDS: Gas drilling; Dual poroelasticity; Tight sandstone; Mudstone; Wellbore stability

INTRODUCTION

The exploration of tight sandstone gas reservoirs in China is still in its infant stage results from a serious of great challenges during conventional exploration well drilling. Several formation damages prevent the timely discovery and accurate evaluation of tight sandstone gas reservoirs, resulting in inaccurate exploratory development strategy. It is well known that gas drilling has the advantages of avoiding formation damages caused by drilling fluid invasion, improving drilling speed, and shortening the well construction period[1-2]. Field trials in Sichuan and Tarim basin indicate enhanced exploration efficiency for tight sandstone gas reservoirs by means of gas drilling. However, wellbore instability is also one of the major contributors to gas drilling problems. In addition to insufficient mud weight, tight sandstone wellbore instability is influenced by gas production from unexpected gas pay zones. In well DX 1 of Tarim basin, unexpected high pressure gas outburst from the fractured tight sandstone gas reservoirs were experienced, which leads to tight sandstone wellbore instability and overlying mudstone collapse, restricting the further development and application of gas drilling.

The influence of gas production on wellbore stability has been widely recognized and some fluid-solid coupling models of wellbore stability have also been developed. Liu et al.[2] found that gas production has a great influence on borehole stability of tight sandstone and overlying mudstone. Kim et al.[3] investigated the wellbore stability from the subsidence results and found that high production rates may lead to large subsidence. Retqvist et al.[4, 5] investigated production performance and geomechanical responses during gas production and indicated that vertical compaction and increased shear stress may cause local yielding of the formation. Zhang et al.[6] presented a coupled model to quantify the change in permeability, the gas flow, and the deformation. They indicated that the sense of permeability change is controlled by the competing influences of effective stresses and sorption-based volume changes. However, previous studies are limited to single-porosity media, and not applicable to dual-porosity media like fractured tight sandstone reservoirs. Liu et al.[7, 8] proposed a dual poroelastic model for gas flow and the resultant deformation, but this is under assumption of no difference between matrix pore pressure and fracture pressure. Wu et al.[9] extended the work of Zhang[6] presented a dual poroelastic model to study the influence of gas sorption induced coal deformation on porosity and permeability. All of these previous models were developed primarily to investigate the gas recovery/injection rates and the gas flow was assumed to observe Darcy law.

Previous studies have improved our understanding of possible causes of wellbore instability caused by gas production, but the effect of gas production on stress redistribution and borehole stability have not been explicitly demonstrated. In this work, first the governing equations of poroelasticity for fractured tight sandstone are introduced. Then the stress and pressure distribution around a borehole in tight sandstone, and the effect of gas production on the stress distribution of overlying mudstone are presented.

GOVERNING EQUATIONS

The coupled poroelastic model are constructed based on the following assumptions: (a) Tight sandstone is a dual poroelastic medium. (b) Strains are infinitesimal. (c) Tight sandstone is saturated by one gas component. (d) The system is isothermal and the gas viscosity is constant. (e) The gas flow observes the non-Darcy law.

Tight sandstone deformation

Based on Terzaghi's generalized effective stress principle, the deformation equation is defined as[10],

$$Gu_{i,jj} + \left(K + \frac{G}{3}\right)u_{j,ji} - \alpha p_{\mathrm{m},i} - \beta p_{\mathrm{f},i} + f_i = 0 \tag{1}$$

where u is the displacement; p_{m} and p_{f} are matrix pore pressure and fracture pressure, respectively; K and G are bulk and shear moduli; α and β are the Biot coefficients of matrix and fracture; f_i is the body force.

Gas flow

The mass balance equation for gas phase under isothermal condition is defined as,

$$\frac{\partial m}{\partial t} + \nabla \cdot \left(\rho_{\mathrm{g}} \vec{u}_{\mathrm{g}}\right) = Q_{\mathrm{g}} \tag{2}$$

where m is the gas content; t is time; ρ_{g} is the gas density; $\vec{u}_{\mathrm{g}}$ is the seepage velocity of gas phase; Q_{g} is the gas source.

Gas density in Eq. (2) is defined as,

$$\rho_{\mathrm{g}} = \frac{pM_{\mathrm{g}}}{ZRT} \tag{3}$$

where p is gas pressure; M_{g} is molecular mass of the gas; R is the universal gas constant; T is the absolute gas temperature; Z is the gas deviation factor.

The influence of turbulence and inertia on high pressure gas production can't be ignored due to the great difference in pressure between bottom-hole and formation during gas drilling. Assuming the effect of gravity can be neglected, and the Forchheimer equation is used to describe the non-Darcy gas flow[12],

$$\vec{u}_{\mathrm{g}} = -\delta \frac{k_{\mathrm{g}}}{\mu_{\mathrm{g}}} \nabla p \tag{4}$$

$$\delta = \frac{1}{1 + \frac{k_{\mathrm{g}}}{\mu_{\mathrm{g}}} \beta_{\mathrm{g}} \rho_{\mathrm{g}} \left|\vec{u}_{\mathrm{g}}\right|} \tag{5}$$

Where μ_{g} is the gas viscosity; k_{g} is the permeability; β_{g} is the characteristic parameter.

Substituting Eqs. (3)-(5) into Eq. (2), one obtains the governing equations for gas flow as follows,

$$\phi_{\mathrm{m}} \frac{\partial p_{\mathrm{m}}}{\partial t} + p_{\mathrm{m}} \frac{\partial \phi_{\mathrm{m}}}{\partial t} + \nabla \cdot \left(-\delta \frac{k_{\mathrm{m}}}{\mu_g} p_{\mathrm{m}} \nabla p_{\mathrm{m}}\right) = -\xi p_{\mathrm{m}} \left(p_{\mathrm{m}} - p_{\mathrm{f}}\right) \tag{6}$$

$$\phi_{\mathrm{f}} \frac{\partial p_{\mathrm{f}}}{\partial t} + p_{\mathrm{f}} \frac{\partial \phi_{\mathrm{f}}}{\partial t} + \nabla \cdot \left(-\delta \frac{k_{\mathrm{f}}}{\mu_{\mathrm{g}}} p_{\mathrm{f}} \nabla p_{\mathrm{f}}\right) = \xi p_{\mathrm{m}} \left(p_{\mathrm{m}} - p_{\mathrm{f}}\right) \tag{7}$$

Where ϕ_{m} and ϕ_{f} are the components of matrix and fracture porosity, respectively; k_{m} and k_{f} are the matrix and fracture permeability, respectively; p_{m} and p_{f} are the matrix pore pressure and fracture pressure, respectively.

ξ is the transfer coefficient between matrix and fracture defined as[9, 11],

$$\xi = \frac{8n}{s^2}\frac{k_{\mathrm{m}}}{\mu_{\mathrm{g}}} \tag{8}$$

where n is the set of normal fractures.

The matrix porosity of the dual porosity medium is defined as[6],

$$\phi_{\mathrm{m}} = \frac{K_{\mathrm{m}}}{K_{\mathrm{m}}\left(1+\varepsilon_{\mathrm{v}}\right)+p_{\mathrm{m}}}\left[\phi_{\mathrm{m0}}+\alpha\left(\varepsilon_{\mathrm{v}}+\frac{p_{\mathrm{m}}-p_{\mathrm{m0}}}{K_{\mathrm{m}}}\right)\right] \tag{9}$$

Where ε_{v} is the volumetric strain; p_{m0} is the initial matrix pore pressure; ϕ_{m0} is the initial matrix porosity.

Then the partial derivative of ϕ_{m} with respect to time can be expressed as,

$$\frac{\partial\phi_{\mathrm{m}}}{\partial t} = \frac{K_{\mathrm{m}}\left(\alpha-\phi_{\mathrm{m}}\right)}{K_{\mathrm{m}}\left(1+\varepsilon_{\mathrm{v}}\right)+p_{\mathrm{m}}}\left(\frac{\partial\varepsilon_{\mathrm{v}}}{\partial t}+\frac{1}{K_{\mathrm{m}}}\frac{\partial p_{\mathrm{m}}}{\partial t}\right) \tag{10}$$

Matrix permeability is concerned with the matrix porosity and grain-size distribution of the porous medium, here the cubic relation between the porosity and permeability is used[9],

$$\frac{k_{\mathrm{m}}}{k_{\mathrm{m0}}} = \left(\frac{\phi_{\mathrm{m}}}{\phi_{\mathrm{m0}}}\right)^3 \tag{11}$$

Where k_{m0} is the initial matrix permeability.

Substituting Eq. (9) into Eq. (11) results in the matrix permeability,

$$k_{\mathrm{m}} = k_{\mathrm{m0}}\left\{\frac{K_{\mathrm{m}}}{K_{\mathrm{m}}\left(1+\varepsilon_{\mathrm{v}}\right)+p_{\mathrm{m}}}\left[1+\frac{\alpha}{\phi_{\mathrm{m0}}}\left(\varepsilon_{\mathrm{v}}+\frac{p_{\mathrm{m}}-p_{\mathrm{m0}}}{K_{\mathrm{m}}}\right)\right]\right\}^3 \tag{12}$$

The change of fracture aperture is defined as[7],

$$\frac{\Delta b}{b_0} = \frac{s_0}{3b_0}\left(1-\frac{E}{E_{\mathrm{m}}}\right)\varepsilon_{\mathrm{v}} \tag{13}$$

The change of porosity of the fracture system can be defined as follows,

$$\frac{\phi_{\mathrm{f}}}{\phi_{\mathrm{f0}}} = \frac{3b/s}{3b_0/s_0} \approx \frac{b_0+\Delta b}{b_0} = 1+\frac{\Delta b}{b_0} \tag{14}$$

Then the fracture porosity then can be obtained by substituting Eq. (13) into Eq. (14),

$$\phi_{\mathrm{f}} = \phi_{\mathrm{f0}} + \frac{E_{\mathrm{m}}\varepsilon_{\mathrm{v}}}{E_{\mathrm{m}}+k_{\mathrm{n}}s} \tag{15}$$

Such that the partial derivative of ϕ_{f} with respect to time can be expressed as,

$$\frac{\partial\phi_{\mathrm{f}}}{\partial t} = \frac{E_{\mathrm{m}}}{E_{\mathrm{m}}+k_{\mathrm{n}}s}\frac{\partial\varepsilon_{\mathrm{v}}}{\partial t} \tag{16}$$

The fracture permeability of the fracture system can be defined as[9, 13],

$$k_{\mathrm{f}}=\frac{b^{3}}{12s}=k_{\mathrm{f0}}\left(1+\frac{1}{\phi_{\mathrm{f0}}}\frac{E_{\mathrm{m}}\varepsilon_{\mathrm{v}}}{E_{\mathrm{m}}+k_{\mathrm{n}}s}\right)^{3} \tag{17}$$

Substituting Eq. (10) into Eq. (6) and Eq. (16) into Eq. (7) yields the final flow equations,

$$\left[\phi_{\mathrm{m}}+\frac{(\alpha-\phi_{\mathrm{m}})p_{\mathrm{m}}}{K_{\mathrm{m}}(1+\varepsilon_{\mathrm{v}})+p_{\mathrm{m}}}+\frac{K_{\mathrm{m}}(\alpha-\phi_{\mathrm{m}})p_{\mathrm{m}}}{K_{\mathrm{m}}(1+\varepsilon_{\mathrm{v}})+p_{\mathrm{m}}}\frac{\partial\varepsilon_{\mathrm{v}}}{\partial p_{\mathrm{m}}}\right]\frac{\partial p_{\mathrm{m}}}{\partial t}+\nabla\cdot\left(-\delta\frac{k_{\mathrm{m}}}{\mu_{\mathrm{g}}}p_{\mathrm{m}}\nabla p_{\mathrm{m}}\right)=-\xi p_{\mathrm{m}}(p_{\mathrm{m}}-p_{\mathrm{f}}) \tag{18}$$

$$\left(\phi_{\mathrm{f}}+\frac{E_{\mathrm{m}}p_{\mathrm{f}}}{E_{\mathrm{m}}+k_{\mathrm{n}}s}\frac{\partial\varepsilon_{\mathrm{v}}}{\partial p_{\mathrm{f}}}\right)\frac{\partial p_{\mathrm{f}}}{\partial t}+\nabla\cdot\left(-\delta\frac{k_{\mathrm{f}}}{\mu_{\mathrm{g}}}p_{\mathrm{f}}\nabla p_{\mathrm{f}}\right)=\xi p_{\mathrm{m}}(p_{\mathrm{m}}-p_{\mathrm{f}}) \tag{19}$$

Therefore, Eqs. (1), (18), (19) define the coupled model for fractured tight sandstone.

BOREHOLE PRESSURE AND STRESS ANALYSIS

Solution strategy

To study the impact of unexpected gas production of tight sandstone on the stress field around the borehole, consider the vertical well DX 1 that drilled as air drilling in Tarim basin as an example. Unexpected high pressure gas production of tight sandstone was experienced when drilling to depth of 4811 m, leading to borehole instability of tight sandstone and the overlying mudstone in the early stage of gas production. This problem was finally removed by motioning the drill pipe up and down. Finite element mesh of the model geometry is shown in Figure 1 and the material properties of tight sandstone and mudstone are shown in Table 1.

Table 1: Parameters used in the example

Parameters	Value
Young's modulus of tight sandstone/mudstone, E	13.2 / 27.8 GPa
Matrix Young's modulus of tight sandstone, E_{m}	32.7 GPa
Possion's ratio of tight sandstone/mudstone, v	0.21/0.26
Equivalent horizontal stress, σ_{e}	99.85 MPa
Vertical stress, σ_{v}	123.10 MPa
Initial permeability of matrix, k_{m0}	2.27×10^{-17} m^2
Initial fracture aperture, b_0	2×10^{-5} m
Initial fracture spacing, s_0	0.02 m
Initial porosity of matrix, ϕ_{m0}	0.06
Initial formation pressure, p_{m0} / p_{f0}	83.54 MPa
Bottom hole pressure, p_{w}	3 MPa
Formation temperature, T	397.15 K
Gas viscosity, μ_{g}	1.84×10^{-5} Pa·s

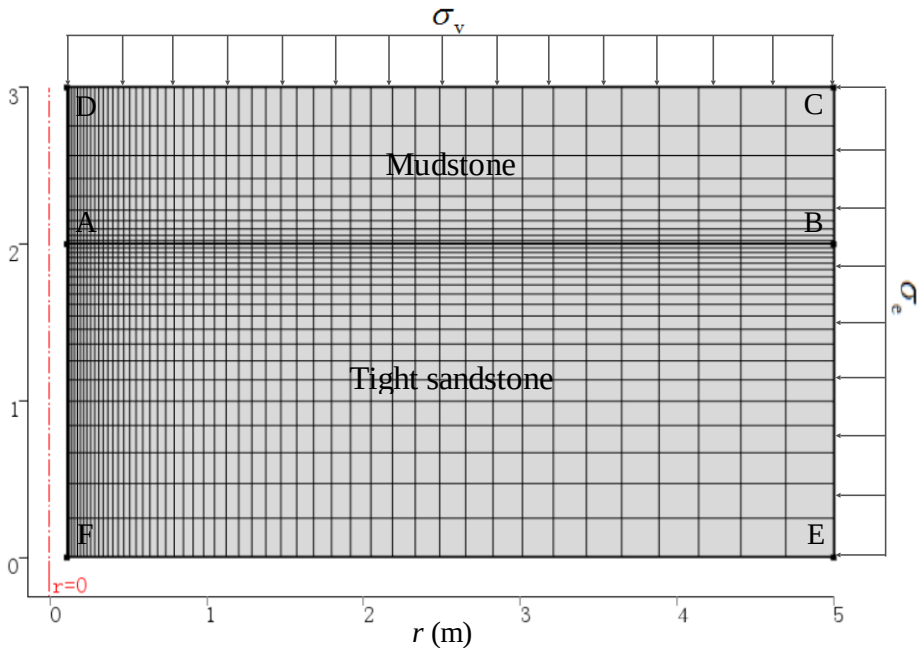

Figure 1: Spatial discretization of the model geometry

In order to avoid inherent computational difficulties, the equivalent horizontal stress (σ_e) is considered, such that the axisymmetric finite element model can be used to solve the field equations and the stresses and pressures are independent on the direction. The equivalent horizontal stress and vertical stress are aligned with the r and z axes, respectively. If gas production of tight sandstone is considered, model ABCD represents mudstone and ABEF tight sandstone, i.e., line AB represents the lithology interface. If gas production is not considered, the whole model represents mudstone for comparison.

Borehole pressure and stress analysis in tight sandstone

Distribution of matrix pressure and fracture pressure of tight sandstone along FE at different time steps (10 s, 60 s and 360 s) is presented in Figure 2. It can be observed that both matrix pressure and fracture pressure sharply drop and fall below the formation pressure near the wellbore. The fracture pressure drop in the near wellbore area is more pronounced than that of matrix pressure, so when the fracture pressure decreases the gas in the matrix flows into the fracture due to gradient. However, away from the wellbore wall the fracture pressure is nearly identical to the matrix pore pressure.

Figure 3 shows the distribution of volumetric strain along FE at different time steps. It reveals that the maximum volumetric strains that result from drilling occur at the borehole well, where the pressure gradient is the highest. Tight sandstone shrinks with decreasing pore pressure and the volumetric strain modification profiles propagate outward from the borehole with time. These changes around a wellbore are driven by gas production rate and pressure decline at the wellbore. As volumetric strain plays an important role in the variation of porosity and permeability, shrinkage of the tight sandstone may result in changes in porosity and permeability.

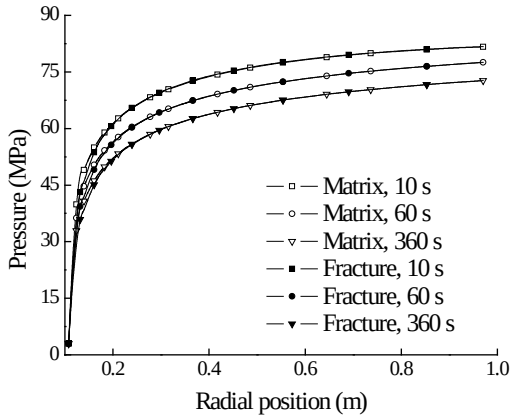

Figure 2: Pressure distribution along FE

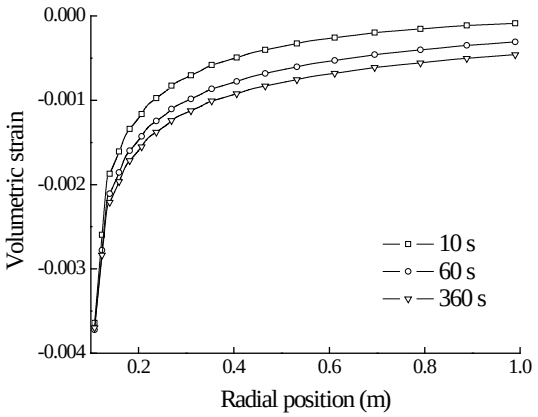

Figure 3: Volumetric strain distribution along FE

The results of matrix and fracture permeability ratio distribution along FE are shown in Figure 4. The permeability ratios decrease with a decrease in pressure (or an increase in effective stress) as expected. For the continuous orthogonal fracture, the fracture permeability is closely related to the size of matrix block and fracture aperture. As the fracture aperture is relatively small, leading to strong stress sensitivity of fracture permeability, thus when the matrix and fracture pressure are reduced, the fracture permeability drops more sharply than that of matrix.

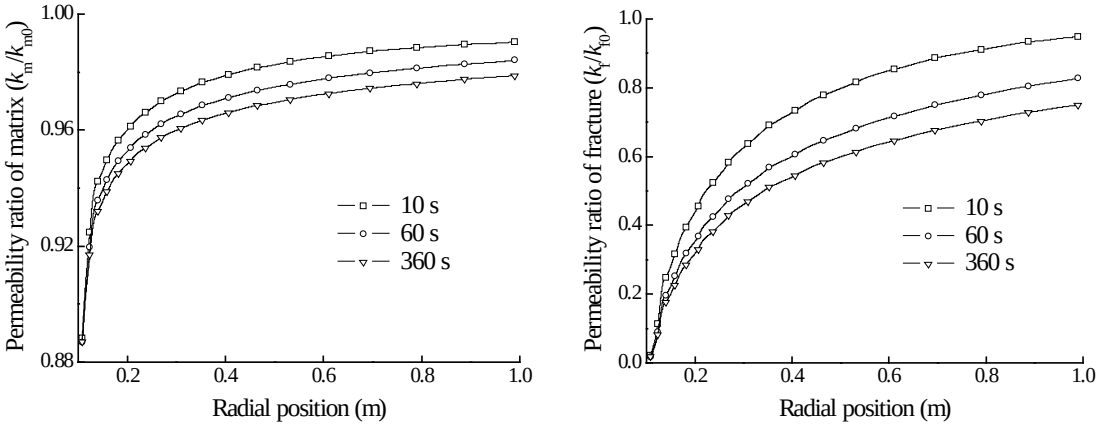

(a) (b)

Figure 4: Permeability radio distribution along FE, (a) matrix; (b) fracture

Figure 5 shows the evolution of effective radial and tangential stresses of the tight sandstone along FE with time, respectively. It is evident that there exists a negative effective radial stress in the near wellbore area results from the great difference between the bottom-hole pressure and the formation pressure. The maximum tensile effective radial stress occurs in the vicinity of the wellbore, which means when the effective radial stress passes beyond the rock tensile strength, exfoliation mode of failure is likely to be experienced. As time passes the effective radial stress increases suggesting enhanced wellbore stability with respect to tensile failure, i.e., wellbore instability is most likely to occur in the early production period of tight sandstone gas formations. This is consistent with the analysis of Liu et al.[2] and field experience. From Figure 5b it can be seen that the effective tangential stress decreases with an increase in distance from the borehole wall, and it increases over time near the wellbore, however, there exists a slight reduction of the hoop stress at the borehole wall.

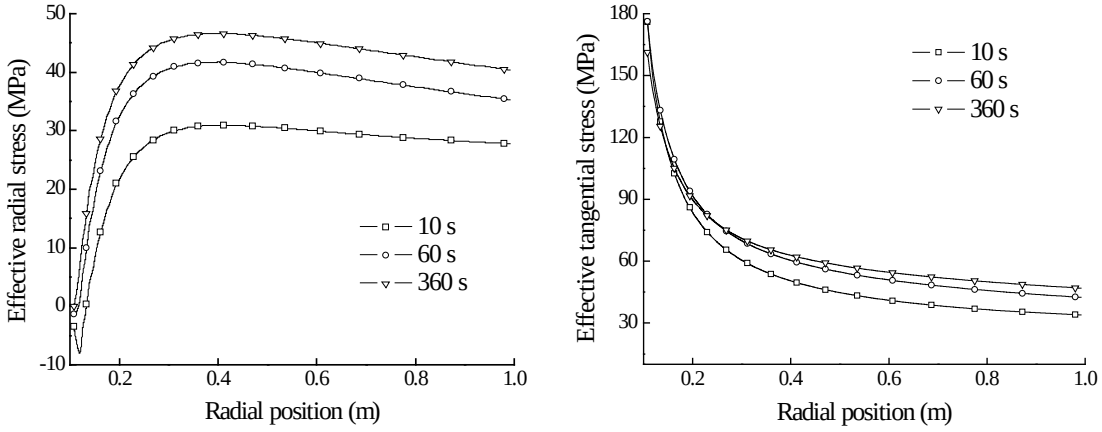

(a) (b)

Figure 5: Stress distribution along FE, (a) effective radial stress; (b) effective tangential stress

The distribution of total radial stress and tangential stress as a function of radial position from the borehole wall is presented in Figure 6. It can be observed that both the total radial stress and tangential stress change with time and space. The total radial stress increases with radial position, while the total tangential stress decreases with radial position. With the passing of time, the total radial stress at the wellbore wall is slightly increased. But overall, reductions in the total radial and tangential stresses of near wellbore are observed. This relaxes the prior assumption that total stresses remain constant during gas production.

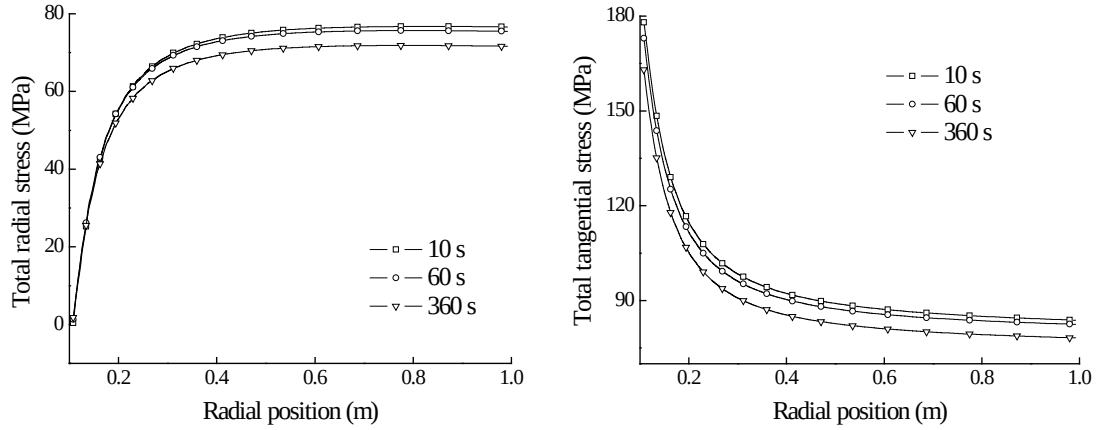

(a) (b)

Figure 6: Stress distribution along FE, (a) total radial stress; (b) total tangential stress

Stress analysis at the borehole wall

In order to investigate the impact of unexpected gas production on stress redistribution of the overlying mudstone, here the total radial and tangential stresses at the borehole wall (FD in Figure 1) are studied. Presented in Figure 7a is the distribution of total radial stress at the borehole wall along z axis. It can be observed that there exists an abrupt change of total radial stress at the lithology interface, and the total radial stress in tight sandstone is smaller than that in mudstone. The results also show that near the lithology interface, the total radial stress in mudstone is slightly elevated, however, away from the lithology interface it is slightly reduced. As time goes on, the total radial

stress in sandstone increases as previously mentioned, whereas it remains relatively unchanged in mudstone.

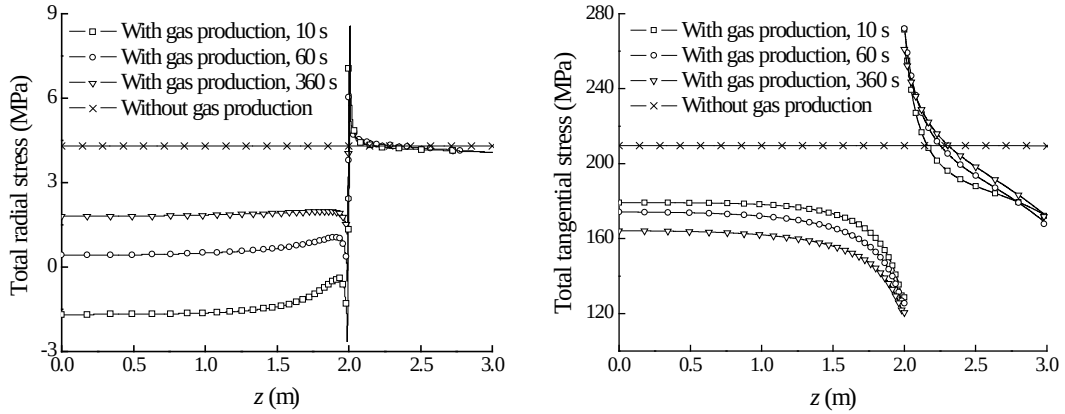

Figure 7: Stress distribution along FD, (a) Total radial stress; (b) Total tangential stress

Figure 7b shows the distribution of total tangential stress at the borehole wall with and without gas production. It is evident that lithology variation tends to reduce the total tangential stress in tight sandstone, while dramatically elevates it in mudstone that adjacent to the lithology interface. This makes the mudstone near the lithology interface become more compressive, increasing the potential for shear failure. However, away from the lithology interface the total tangential stress in mudstone is significantly reduced, suggesting enhanced wellbore stability with respected to shear failure.

Figure 8 presents the distribution of the volumetric strain at the borehole wall (FD in Figure 1). It reveals that the volumetric strain of mudstone is largely increased by gas production. In spite of the continuous displacement at the lithology interface, volumetric strain in tight sandstone is different from that of mudstone as a result of gas production from tight sandstone gas formation.

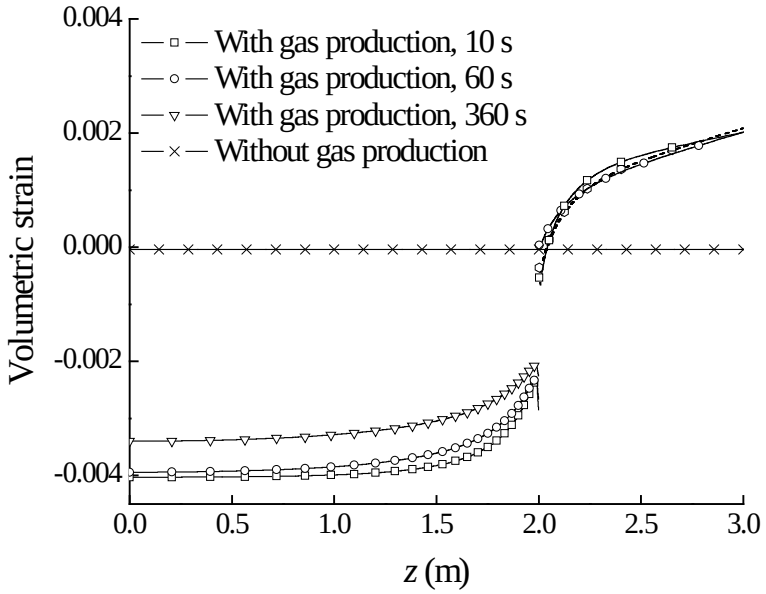

Figure 8: Volumetric strain distribution at the borehole wall (FD)

CONCLUSIONS

(1) A coupled poroelastic model for fractured tight sandstone is developed to quantify the change in permeability, the non-Darcy gas flow, and the deformation. The coupling between gas flow and tight sandstone deformation is realized through the matrix/fracture porosity and permeability models. Then the pressure and prevailing stress distributions around a borehole in fractured tight sandstone have been studied and the impact of high pressure gas production on stress distribution in the overlying mudstone has also been investigated.

(2) The pressure analysis shows that the fracture pressure drops more obvious than that of matrix pressure. The stress analysis shows that tight sandstone can experience the exfoliation mode of failure as a result of negative effective radial stress near the wellbore wall. Gas production generally tends to increase the effective radial and tangential stresses, suggesting enhanced the tight sandstone wellbore stability with respect to tensile failure.

(3) Lithology variation makes the total radial and tangential stresses change abruptly at the lithology interface, i.e., the total radial stress in the overlying mudstone is slightly elevated, while the total tangential stress is largely increased, which means the overlying mudstone is likely to undergo shear failure and gas production will further deteriorate the mudstone wellbore stability.

ACKNOWLEDGEMENTS

The research is supported by the Sichuan Provincial Development Scheme for the Leaders of Disciplines in Science (No. 2014JQ0045) and Innovative Research Team Foundation of Sichuan Provincial Universities (No. 2014TD0006).

REFERENCES

1. Zhang H, Zhang H, Guo B, et al. Analytical and numerical modeling reveals the mechanism of rock failure in gas UBD[J]. *Journal of Natural Gas Science and Engineering*. 2012, 4(1): 29-34.
2. Liu H, Meng Y, Wan S. et al. Analysis of wellbore stability during gas drilling through high pressure gas formations[J]. Natural Gas Industry, 2010, 30(11): 59-62.
3. Kim J, Moridis G J, Rutqvist J. Coupled flow and geomechanical analysis for gas production in the Prudhoe Bay Unit L-106 well Unit C gas hydrate deposit in Alaska[J]. *Journal of Petroleum Science and Engineering*, 2012, 92(1): 143-157.
4. Rutqvist J, Moridis G J, Grover T, et al. Geomechanical response of permafrost-associated hydrate deposits to depressurization-induced gas production[J]. *Journal of Petroleum Science and Engineering*, 2009, 67(1): 1-12.
5. Rutqvist J, Moridis G J, Grover T, et al. Coupled multiphase fluid flow and wellbore stability analysis associated with gas production from oceanic hydrate-bearing sediments[J]. Journal of Petroleum Science and Engineering, 2012, 92(1): 65-81.
6. Zhang H, Liu J, Elsworth D. How sorption-induced matrix deformation affects gas flow in coal seams: a new FE model[J]. *International Journal of Rock Mechanics and Mining Sciences*. 2008, 45(8): 1226-1236.
7. Liu J, Chen Z, Elsworth D, et al. Evaluation of stress-controlled coal swelling processes[J]. *International Journal of Coal Geology*. 2010, 83(4): 446-455.

8. Liu J, Chen Z, Elsworth D, et al. Linking gas-sorption induced changes in coal permeability to directional strains through a modulus reduction ratio[J]. *International Journal of Coal Geology*. 2010, 83(1): 21-30.

9. Wu Y, Liu J, Elsworth D, et al. Dual poroelastic response of a coal seam to CO2 injection[J]. *International Journal of Greenhouse Gas Control*. 2010, 4(4): 668-678.

10. Wilson R K, Aifantis E C. On the theory of consolidation with double porosity[J]. *International Journal of Engineering Science*. 1982, 20(9): 1009-1035.

11. Kazemi H, Gilman J R. Multiphase flow in fractured petroleum reservoirs[J]. Flow and Contaminant Transport in Fractured Rock. 1993, 6(1): 267-323.

12. Choi E S, Cheema T, Islam M R. A new dual-porosity/dual-permeability model with non-Darcian flow through fractures[J]. *Journal of Petroleum Science and Engineerin*g. 1997, 17(3): 331-344.

13. Robertson E P, Christiansen R L. A permeability model for coal and other fractured sorptive-elastic media[J]. *SPE Journal*. 2008, 13(3): 314-324.

14. Tianshou Ma and Ping Chen: "Wellbore Stability Analysis of Inclined Wells in the AY Field" *Electronic Journal of Geotechnical Engineering*, 2015 (20.4) pp 1313-1329. Available at ejge.com.

Editor's note.
This paper may be referred to, in other articles, as:

Xu Yang, Yingfeng Meng, Gao Li, Hanfeng Tang, Liang Wang: "Analysis of Stress Distribution around a Wellbore Drilled in Tight Sandstone Formations during Gas Drilling" *Electronic Journal of Geotechnical Engineering*, 2016 (21.12), pp 4495-4505. Available at ejge.com.